# Accepted Manuscript

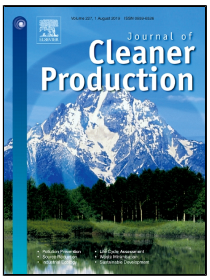


Modeling of hydrate-based $CO_2$ capture with nucleation stage and induction time prediction capability

Hossein Dashti, Daniel Thomas, Amirpiran Amiri

| | |
|---|---|
| PII: | S0959-6526(19)31774-3 |
| DOI: | 10.1016/j.jclepro.2019.05.240 |
| Reference: | JCLP 17005 |
| To appear in: | *Journal of Cleaner Production* |
| Received Date: | 31 March 2019 |
| Accepted Date: | 21 May 2019 |

Please cite this article as: Hossein Dashti, Daniel Thomas, Amirpiran Amiri, Modeling of hydrate-based $CO_2$ capture with nucleation stage and induction time prediction capability, *Journal of Cleaner Production* (2019), doi: 10.1016/j.jclepro.2019.05.240

# Modeling of hydrate-based $CO_2$ capture with nucleation stage and induction time prediction capability

**Hossein Dashti[a], Daniel Thomas[b], Amirpiran Amiri*[,b]**

[a] WA School of Mines: Minerals, Energy and Chemical Engineering, Curtin University, Kent Street, Bentley WA 6102, Australia

[b] European Bioenergy Research Institute (EBRI), School of Engineering and Applied Science, Aston University, Birmingham, B4 7ET, United Kingdom

*Corresponding Authors: a.p.amiri@aston.ac.uk

## Abstract

Gas hydrate technology is a promising approach for carbon capture. However, due to the multi-physics and multi-scale complexity of the process, this technology is not sufficiently understood for real-life scale applications. In particular, further fundamental studies of the hydrate formation mechanisms and rate are needed to achieve relevant insights into the process design and intensification. High-fidelity numerical models are crucial to capture and explain the dominant physicochemical mechanisms involved in the process. This paper presents a new variation of the shrinking core model (SCM) that can capture the practically observed features of the carbon dioxide ($CO_2$) hydration process, including the nucleation phase behavior and induction time, which have not been exploited previously. Accordingly, the most significant contribution of the current work to the literature is the proposal and demonstration of an efficient and rapid predictive tool for the $CO_2$ hydrate nucleation process. Moreover, a model-based estimation of the induction time, as a critical parameter in $CO_2$ hydrate rate estimation and control, is presented. Additionally, the temperature history profile over the nucleation and growth phases is simulated and compared against experimental data from the literature. The proposed model offers an in-depth and rationale analysis tool compared to the primary forms of the SCM and other models in which the nucleation stage has been compromised for the sake of mathematical modeling and numerical solution simplicity. The proposed concept is generic enough to be used for $CH_4$ hydration process too.

**Keywords:** $CO_2$ capture, gas hydrate, nucleation, shrinking core model, induction time

## 1. Introduction

Clathrate gas hydrates are small, solid crystalline, ice-like structures formed at high-pressure and low-temperature conditions via van der Waals interactions of water molecules in the

hydrate lattice and gas molecules (Englezos, 1993). Many gases such as methane ($CH_4$), carbon dioxide ($CO_2$), ethane ($C_2H_6$), nitrogen ($N_2$) and hydrogen sulfide ($H_2S$) are capable of forming gas hydrates. Applications of hydrate technology in the separation and storage of gases such as $CH_4$ and $CO_2$ and desalination have been reported in the literature (Dashti and Lou, 2018; Dashti et al., 2015; Sloan and Koh, 2008). Under appropriate thermodynamic conditions, the amount of gas inside the hydrated crystals can reach up to 170 times more than that feasible under standard thermodynamic conditions (Selim and Sloan, 1989). At a pressure higher than 4.5 MPa and a temperature lower than 283 K, $CO_2$ forms a hydrate structure, $CO_2 \cdot nH_2O$, where $n$=5.75 assuming full occupancy of the water cages (Sloan and Koh, 2008; Sun and Kang, 2016). Under these conditions, the solubility of $CO_2$ in water is approximately 0.031 mole $CO_2$/mole $H_2O$ (Diamond and Akinfiev, 2003). Feasible $CO_2$ capture in water may increase by fivefold through hydration. Unique features such as the moderate operational temperature range, low energy consumption and capability for continuous operation have made gas hydrate technology one of the promising approaches for $CO_2$ capture and separation (Dashti et al., 2015). Extensive research has focused on the thermodynamics of the gas hydrate formation process (Eslamimanesh et al., 2012). Experimental investigations of $CO_2$ hydrate formation mechanisms have also been widely reported (Clarke and Bishnoi, 2005; Dashti and Lou, 2018; Teng et al., 1995; Uchida et al., 1999; Yang et al., 2011; Yin et al., 2018). However, an insightful understanding of the complex fundamentals of the process, such as nucleation, is still needed for the gas hydrate-based $CO_2$ capture (HBCC) process to become technically and economically viable at large scales.

The process of gas hydrate formation includes two main steps: hydrate nucleation and growth. Based on concepts of crystallization, the availability of a supersaturated condition does not necessarily guarantee the initiation of the crystallization process; solid nucleate particles must exist in the solution (Mullin, 2001). Sloan and Koh defined the “nucleation” stage as the process in which small cluster particles of the gas and water molecules initiate, grow and dissolve in order to reach a critical cluster size (Sloan and Koh, 2008). Khurana et al. reported that the classical nucleation approach is insufficient to reveal the exact pathway of the nucleation process as well as the hydrate structures (Khurana et al., 2017).

Measurement of nucleation phase behavior through experimental investigations is very difficult and complicated due to the stochastic and sudden appearance of this phase (Ripmeester and Alavi, 2016). The nucleation stage is followed by the so-called “growth” stage in which a considerable increase in gas uptake occurs, and gas hydrate formation can be controlled by

pseudo-reaction intrinsic kinetics, heat or mass transfer phenomena or a combination thereof (Sloan and Koh, 2008). The roles played by these phenomena might be greatly affected by the nucleation process and variations in nucleate phase properties. Experimentally, it is challenging to capture the time-dependent variations of the nucleation process, which emphasizes the importance of numerical simulation as an alternative to further understanding this intermediate stage.

Current models for the gas hydration and nucleation processes are mostly based on thermodynamic concepts. Chemical potential (Skovborg et al., 1993), fugacity (Natarajan et al., 1994), and temperature (Vysniauskas and Bishnoi, 1983) variations are key variables used in hydrate modeling in the literature as driving forces to explain hydrate behavior. The modeling scale and methodology vary depending on the modeling target. The molecular simulation approach, for instance, is widely used in the literature to investigate gas hydrates at the nanoscale (English and MacElroy, 2015). Molecular simulations describe the nucleation process as a two-step process in which disordered crystal-like structures form and then are converted to more detectable crystalline forms of particles (Jacobson et al., 2010a). A critical challenge associated with molecular-level simulations is the time-consuming computations because of the slow processes, which include gas diffusion into the liquid phase and heat transfer during the formation of nucleate particles (English and MacElroy, 2015). To avoid large simulation timescales in the nucleation process, most studies have attempted to use a high driving force, which is not representative of the real experimental and industrial settings of the nucleation process (Walsh et al., 2011). Similar challenges and pitfalls are present when modeling of the gas hydrate growth phase is attempted (Ribeiro Jr and Lage, 2008).

Solid-fluid models are another approach to model the process of gas hydrate formation. The unreacted shrinking core model (SCM), in particular, has been commonly used for modelling of gas-solid reactions in which the diffusion rate is slow compared to the reaction rate on the unreacted core (Amiri et al., 2015). It has been shown that diffusion in the hydrate layer, in contrast to the mass transfer in the fluid surrounding the particle, is the most dominant controlling mechanism for the overall progress of $CO_2$ hydration (Dashti et al., 2019). Even though agitation in the reactor positively influences the mass transfer rate in the particle surroundings, it would not have such an impact on the rate of diffusion inside the reacting particle. Accordingly, the controlling role of the diffusion mechanism remains significant in explaining the applicability of SCM in both batch and stirred tank reactors modelling.

In SCM, the initial reaction occurs at the outer radius of the solid particle, and then the zone of the reaction moves into the core. As conversion proceeds, the size of the unreacted core decreases. Shi et al. proposed a variation of SCM to simulate gas hydrate growth in the presence of condensate oil in the flow loop (Shi et al., 2011) that incorporated the kinetic model developed by Englezos et al. (Englezos et al., 1987). The authors used experimental data to optimize the kinetic controlling parameters (gas diffusivity, porous property, and mass transfer efficiency). This model was further developed to study the growth kinetics of the methane hydrates in the presence of dry water and porous hydrogel particles (Shi et al., 2014; Shi et al., 2017). Falenty et al. supported the applicability of SCM for $CO_2$ hydrate formation from ice powders using cryo-scanning electron microscopy images (Falenty et al., 2013). While all of these studies have demonstrated the effectiveness of SCM for the prediction of $CO_2$ hydrate growth, none have investigated aspects of hydrate nucleation.

The Englezos model integrates the crystallization and mass transfer theories to describe hydrate crystal growth (Englezos et al., 1987). According to this model, hydrate particle growth involves two sequential steps: (1) diffusion of gas molecules from the bulk solution of gas to the hydrate-water interface and (2) hydration reactions at the interface. The second step is an adsorption process involving the incorporation of gas molecules into water molecules and subsequent stabilization of the structured water. The driving force in this model is the difference between the fugacity of the dissolved gas and the three-phase equilibrium fugacity. The hydrate nucleation stage significantly affects the hydration history profiles, gas concentration, and temperature profiles, based on numerous experimental studies (Khurana et al., 2017; Mullin, 2001; Natarajan et al., 1994; Vatamanu and Kusalik, 2010). It is evident that an understanding of nucleation phase behavior and induction time variations requires nucleation experiments with a complex design. Numerical studies can provide invaluable insights on this stage of the process. Previous modeling studies have mostly focused on either the $CO_2$ hydrate growth phase (Yin et al., 2018) or the microscale phenomena of $CO_2$ nucleation formation conditions at microsecond timescales via molecular simulation (He et al., 2017; Khurana et al., 2017). From the reactor design and optimization perspective, however, a mesoscale model must be integrated with a macroscale (reactor) model that considers mass and heat transport barriers.

In this paper, a new variation of the SCM with modifications to the reported work by Amiri et al. (Amiri et al., 2013b) is developed to describe gas hydrate formation. The model captures both the mass transfer and heat transfer involved in the hydrate formation process and provides

a simulated temperature profile and gas consumption profile that are similar to the reported experimental results. The new model consists of two stages to simulate both the nucleation and growth of the gas hydrates. The most significant contribution of the current work is to propose and demonstrate an efficient and fast predictive tool for the nucleation process as part of a whole $CO_2$ hydration process. Moreover, a model-based estimation of the induction time, as a critical parameter in $CO_2$ hydrate rate estimation and control, is presented. Table 1 provides a comparison of recent $CO_2$ hydrate modeling studies in the open literature with the present work.

Table 1. Comparison of recent $CO_2$ hydrate modeling studies and the current study.

| **Features** | **Contributions** | | | | |
|---|---|---|---|---|---|
| | (Falenty et al., 2013; Henning et al., 2000; Staykova et al., 2003) | (Mochizuki and Mori, 2006; Mori, 2001; Uchida et al., 1999; Uddin et al., 2008) | (Kvamme et al., 2004; Radhakrishnan and Trout, 2002) | (Bai et al., 2011, 2012) | This work |
| Application of SCM in $CO_2$ hydrates | * | – | – | – | * |
| Model-based induction time prediction | – | – | – | * | * |
| Modeling of the nucleation stage | – | – | * | * | * |
| Non-isothermal modeling | – | * | – | – | * |

**Notations:** Considered (*), Not considered (–)

## 2. Multi-stage SCM development

A multi-stage SCM (MSSCM) is proposed and used in this study to capture the features relevant to the nucleation and growth stages, especially the effects of transient control factors. The model is established based on work by Amiri et al. on the simulation of the calcination process in which the gas product inhibits the reaction and a solid intermediate product also forms (Amiri et al., 2013a; Amiri et al., 2015). In an effectively agitated reactor with a constant supply of $CO_2$ gas molecules, as reported by Linga et al., (Linga et al., 2007) hydrate formation is considered to occur in individual water droplets, and therefore the MSSCM encompassing both the nucleation and growth steps can be schematically illustrated as shown in Fig. 1. Nucleation occurs at Stage 1, and there is no hydrate formation/growth during this stage. Further progress of the process in Stage 2 results in the initial growth of gas hydrates, with the formation of the first layer of hydrates. At this stage, nucleation continues while growth of hydrates also occurs. At the end of Stage 2, the fresh water is fully consumed, leaving either nucleate or hydrate behind. At Stage 3, rapid hydrate growth occurs and converts all nucleates to the $CO_2$ hydrate. There is no new nucleate formation at Stage 3. The following assumptions have been applied in the current model:

1. The water droplet is initially pure and spherical with a constant radius throughout the process.
2. When the process starts, the reactor pressure and temperature are 3.25 MP and 270 K, respectively. At this time, $CO_2$ dissolution begins.
3. $CO_2$ dissolution was assumed to be included in the nucleation processes. Therefore, the induction time refers to the time needed to allow $CO_2$ accumulation – via dissolution and nucleation – to reach a critical level sufficient for hydrate formation. The contribution of the dissolution term in overall model performance was examined as presented in the model analysis part.

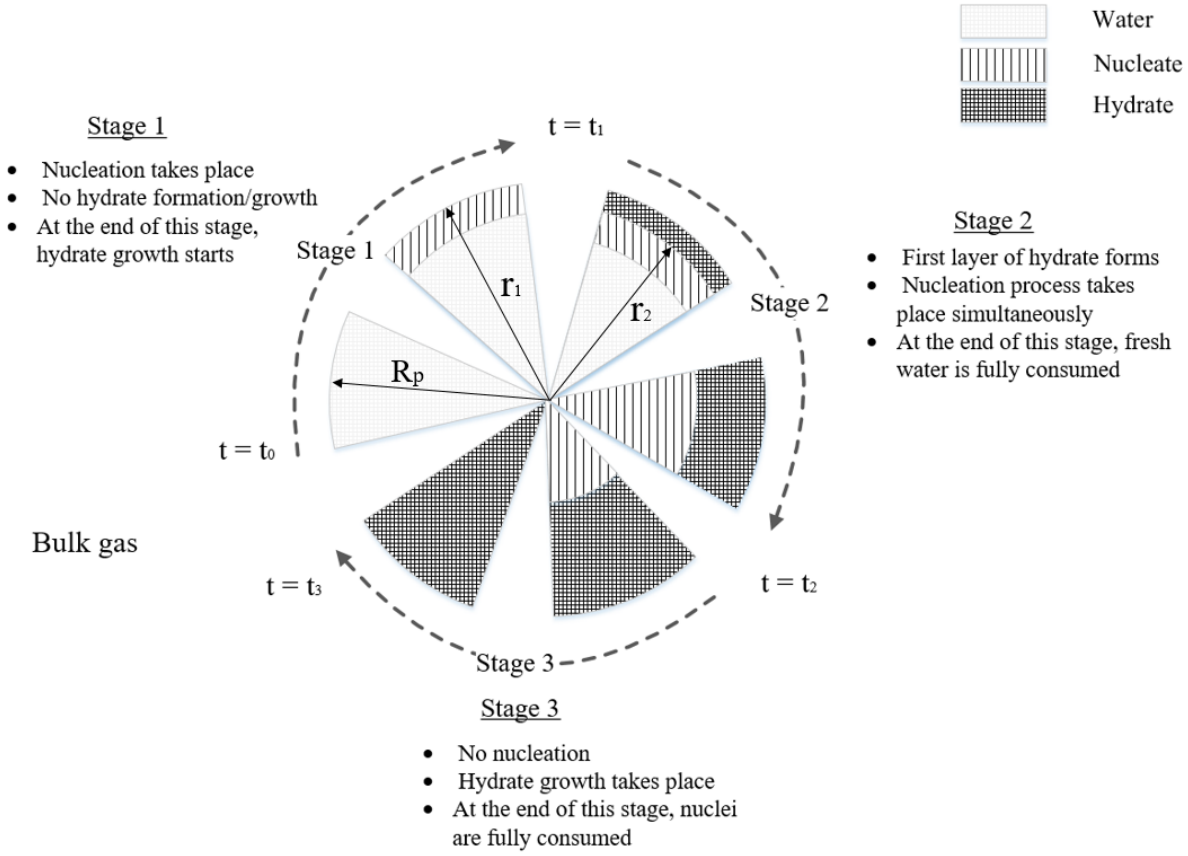


Fig. 1. Schematic of the multi-stage-multi-reaction model for the $CO_2$ hydration process with spherical geometry ($r_1 = r^{W.N}$, $r_2 = r^{N.H}$)

For the formation of $CO_2$ hydrates, the overall reaction is expressed by Eq. (1).

$$CO_2 + nH_2O \xrightarrow{k_1} CO_2 \cdot nH_2O \qquad r_h = k_1 C_{CO_2} \qquad (1)$$

in which $C_{CO_2}$is the $CO_2$ local concentration and $k_1$ is the reaction rate constant.

In this model, an intermediate nucleate ($N$ or $CO_2 \cdot mH_2O$) stage is considered over the pathway to $CO_2$ hydrate ($H$ or $CO_2 \cdot nH_2O$) product, expressed as the following:

$$mH_2O_{(aq)} + CO_{2\,(aq)} \xrightarrow{k_2} N_{(s)} \qquad r_W = k_2 C_{CO_2}^{W.N} \qquad (2)$$

$$N_{(s)} + \alpha CO_{2(aq)} \xrightarrow{k_3} (\alpha + 1)H_{(s)} \qquad r_N = k_3 C_{CO_2}^{N.H} \qquad (3)$$

where $k_2$ and $k_3$ are the reaction rate constants in Eq. (2) and Eq. (3) and $m = (1 + \alpha)n$. $C_{CO_2}^{W.N}$ and $C_{CO_2}^{N.H}$ are the $CO_2$ concentrations at the water/nucleate ($W.N$) and nucleate/hydrate ($N.H$) interfaces, respectively. The multi-stage hydration model governing equations and their derivation details are presented in Table 2 and the Appendix**,** respectively. The initial and boundary conditions are the variables' values at the stages' interface (variables subscripted with 12 and 23 for stage 1 to 2 and 2 to 3 exchanges, respectively). As the two subsequent stages provide the same concentration and temperature at the interface, the stage exchange time is estimated by equating the stages in the models.

Table 2. Model equations for the multi-stage gas hydrate nucleation and growth stages

| Stage | Equations | Initial conditions |
|---|---|---|
| 1 | $1 - \frac{C_{CO_2}^{W.N}}{C_{CO_2}^{b}}\left(1 + \frac{\vartheta_1 k_2 R_p}{D_{e,1}}\left(\frac{r_1}{R_p}\right)^2\left(\frac{1}{\left(\frac{r_1}{R_p}\right)} - 1\right)\right) = 0$ | |
| | $\frac{dr_1}{dt} = -\frac{MW_{H_2O}}{\rho_{H_2O}} k_2 C_{CO_2}^{W.N}$ | $r_1 = R_p$ at $t = t_0$ |
| | $\frac{dT}{dt} = \frac{h(T_b - T) - \left(\frac{r_1}{R_p}\right)^2 k_2 \Delta H_2 C_{CO_2}^{W.N}}{\frac{R_p \rho_{H_2O}}{3MW_{H_2O}} C_{p,1}}$ | $T = T_b$ at $t = t_0$ |
| 2 | $\frac{C_{CO_2}^{N.H}}{C_{CO_2}^{b}} - \frac{C_{CO_2}^{W.N}}{C_{CO_2}^{b}}\left(1 + \frac{\vartheta_1 k_2 R_p}{D_{e,2}}\left(\frac{r_1}{R_p}\right)^2\left(\frac{1}{\left(\frac{r_1}{R_p}\right)} - \frac{1}{\left(\frac{r_2}{R_p}\right)}\right)\right) = 0$<br>$1 - \frac{C_{CO_2}^{N.H}}{C_{CO_2}^{b}} - \left(\frac{\vartheta_1 k_2 R_p C_{CO_2}^{W.N}}{D_{e,2}\ C_{CO_2}^{b}}\left(\frac{r_1}{R_p}\right)^2 + \frac{\vartheta_2 k_3 R_p C_{CO_2}^{N.H}}{D_{e,2}\ C_{CO_2}^{b}}\left(\frac{r_2}{R_p}\right)^2\right)\left(\frac{1}{\left(\frac{r_2}{R_p}\right)} - 1\right) = 0$ | |
| | $\frac{dr_1}{dt} = -\frac{MW_{H_2O}}{\rho_{H_2O}} k_2 C_{CO_2}^{W.N}$ | $r_1 = r_{12}$ at $t = t_1$ |

| | | |
|---|---|---|
| | $\frac{dr_2}{dt} = -\frac{MW_N}{\rho_N} k_3 C_{CO_2}^{N,H}$ | $r_2 = R_p$ at $t = t_1$ |
| | $\frac{dT}{dt} = \frac{h(T_b - T) - \left(\frac{r_1}{R_p}\right)^2 k_2 \Delta H_2 C_{CO_2}^{W,N} - \left(\frac{r_2}{R_p}\right)^2 k_3 \Delta H_3 C_{CO_2}^{N,H}}{\frac{R\rho_{avg,2}}{3MW_{avg,2}} C_{p,2}}$ | $T = T_{12}$ at $t = t_1$ |
| 3 | $1 - \frac{C_{CO_2}^{N,H}}{C_{CO_2}^{b}}\left(1 + \frac{\vartheta_2 k_3 R_p}{D_{e,3}}\left(\frac{r_2}{R_p}\right)^2\left(\frac{1}{\left(\frac{r_2}{R_p}\right)} - 1\right)\right) = 0$ | |
| | $\frac{dr_2}{dt} = -\frac{MW_N}{\rho_N} k_3 C_{CO_2}^{N,H}$ | $r_2 = r_{23}$ at $t = t_2$ |
| | $\frac{dT}{dt} = \frac{h(T_b - T) - \left(\frac{r_2}{R_p}\right)^2 k_3 \Delta H_3 C_{CO_2}^{N,H}}{\frac{R_p\rho_{avg,3}}{3MW_{avg,3}} C_{p,3}}$ | $T = T_{23}$ at $t = t_2$ |

## 3. Model solution and validation

The Matlab *ode23* solver tool was used to numerically solve the set of ordinary differential equations in Table 2. Due to the complex nature of the nucleation phase, the uncertainty in its physical parameters is a real challenge. For the numerical solution (Table 3), the nucleate parameters were assumed based on the fact that the nucleation stage is a precursor stage to the hydration stage and is comprised of cages not fully occupied by the $CO_2$ molecules or semi-formed cages. Therefore, average values of water and hydrates were initially assumed for the nucleate physical properties. For instance, the molecular weight ($MW_N$) and the density ($\rho_N$) of nucleates were assumed to be the average value between the molecular weight and density of water and the $CO_2$ hydrates. The nucleation number ($m$) was assumed as 10, and different values of the nucleation number were used in the model parametric analysis. The $CO_2$ concentration in the bulk gas ($C_{CO_2}^{b}$) was estimated using the Peng-Robinson equation of state (Robinson and Peng, 1978) at a temperature of 270 K (Liang et al., 2016) and pressure of 3.25 MPa.

The effective diffusivities ($D_e$) was estimated as the phase portion-based average value of the diffusivity of the hydrate and nucleate phases. For example, the effective diffusivity in the first stage ($D_{e,1}$) is the average of the diffusivity of the nucleate and the water and changes with the

change in the thickness of the nucleated layer with time. The effective $CO_2$ diffusivity coefficient values in gas hydrates were selected based on the reported values in the literature, which range from $1.0 \times 10^{-14}$ m$^2$/s to $2.0 \times 10^{-16}$ m$^2$/s (Liang et al., 2016).

The reaction rate coefficient $k$ values are reportedly affected by the hydrate surface areas measured in the experiments (Yin et al., 2018). Values on the order of $10^{-5}$ to $10^{-8}$ are reported in different studies (Bergeron and Servio, 2008; Hashemi et al., 2007; Ou et al., 2016). In this study, however, we observed that $k$ values in this range result in a very small Thiele modulus (<<1) indicating that there is almost no role for the reaction rate in controlling the process. This observation is not consistent with previous studies reporting the intrinsic reaction rate as the second controlling mechanism (Sloan and Koh, 2008). We therefore used $k$ values on the order of $10^{-2}$ to conduct a meaningful parametric study, while more precise measurements, particularly for the nucleation reaction, are needed through experimental studies and parameter tuning optimization.

Table 3. Parameters used for MSSCM solution for the $CO_2$ hydration process

| **Parameter** | **Value** |
|---|---|
| $C^b_{CO_2}, mol/m^3$ | 2063.1 |
| $D_{e,1}, m^2/s$ | $8.00\times10^{-14}$ |
| $D_{e,2}, m^2/s$ | $4.04\times10^{-14}$ |
| $D_{e,3}, m^2/s$ | $7.80\times10^{-16}$ |
| $k_2, m/s$ | $9.0 \times10^{-2}$ |
| $k_3, m/s$ | $1.5 \times10^{-3}$ |
| $\Delta H_2, KJ/kg$ | – 20.61 (Lirio and Pessoa, 2013) |
| $\Delta H_3, KJ/kg$ | – 40 (Lirio and Pessoa, 2013) |
| $MW_{H_2O}, g/mol$ | 18 |
| $MW_N, g/mol$ | 404 |
| $n$ | 5.75 (Sun and Kang, 2016) |
| $R_p, m$ | $8.29\times10^{-7}$ |
| $\vartheta_1\ (=m)$ | 10 |
| $\vartheta_2\ (=n/(m-n))$ | 0.4 |
| $\rho_{H_2O}, kg/m^3$ | 1000 |
| $\rho_N, kg/m^3$ | 1050 |

For the estimation of the stage change characteristics, such as time for induction, the fact that the model variables including r, $C_{CO_2}$ and T remain the same in both phases (stages) is considered. The same approach was used to identify the time when Stage 2 shifts to 3.

The model-based time-dependent mass fraction profiles of water, nucleate, hydrate, and experimentally measured gas uptake data (Linga et al., 2007) are presented in Fig. 2. It is impossible to obtain internal particle insights experimentally to validate the particle composition. However, the trajectory of the particle gas uptake behavior achieved via the model agrees well with the experimental trend, thus validating the modeling strategy. The experimentally reported $CO_2$ uptake is based on the bulk gas concertation change over time and provides no insight on the amount of water consumed. This explains the observed deviation between the absolute values of $CO_2$ uptake in the model and experiment (Fig. 2).

The results in Fig. 2(A) show that at the first stage ($t_0/t_{max}$= 0 to $t_1/t_{max}$= 0.18), the nucleation process consumes water and produces nucleate without hydrate formation. This corresponds to the time period in which slow gas uptake is frequently observed in the experimental graphs (Fig. 2(B)). At the end of this stage, the nucleate fraction reaches the maximum value. A decline starts due to the commencement of hydrate growth from critically sized nucleates, indicating the beginning of Stage 2, at $t_1/t_{max}$= 0.18. This stage involves both nucleation and initial rapid growth of hydrates, resulting in the formation of the hydrate shell. The rapid $CO_2$ hydrate growth is indicated by the increase in the hydrate mass fraction. This stage corresponds to the gas uptake observed in the experimental results ($t_1/t_{max}$= 0.18 to $t_2/t_{max}$ = 0.72). Stage 2 finishes at $t_2/t_{max}$= 0.72, which is estimated using the point at which fresh water is fully consumed. During Stage 3, the remaining nucleate is converted to the hydrate. The rate of mass fraction changes during this stage is slow compared to the other stages, principally due to the mass transfer and heat transfer limitation, and the slow driving force will result in slow hydrate formation. Finally, at the end of this stage, the mass fraction rate of the hydrate approaches 1.

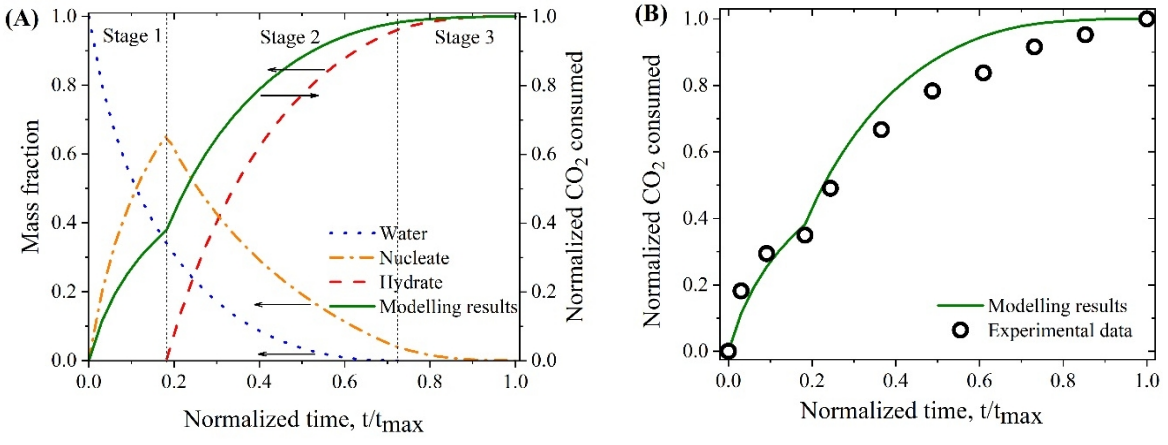

Fig. 2. Results of multi-stage gas hydrate nucleation and growth for the basis case simulation: (A) stages, phases distribution, and gas uptake; (B) comparing modeling results with experimental gas uptake data for the $CO_2/N_2$ system from Linga et al. (Linga et al., 2007).

The nucleation and the growth stage results have been validated against the experimental data using the practically observed trends. The current model prediction compares reasonably with the principal gas consumption trends presented in the literature. The gas consumption and water conversion trends are exchangeable using the hydration number. The experimental data were taken from Linga et al., who reported a series of experimental works on $CO_2/N_2$ hydrate formation (Linga et al., 2007). The operating pressure in the study was much lower than that thermodynamically needed for $N_2$ hydrate formation. It is reasonable to assume that no nitrogen hydrate formation occurs and that there is no interference from the presence of nitrogen in this work. Further, the authors reported that the $CO_2$ content in the hydrate phase increases as the experiment progresses. For example, at a sampling time of 16 min the $CO_2$ fraction in the hydrate phase is 0.87 mole fraction while at a sampling time of 128 min, it is about 0.89 mole fraction. Therefore, it is evident that the hydrate phase is enriched with the $CO_2$ rather than $N_2$.

Since model results are based on a single particle and experimental results are based on an unknown number of particles, we have considered a dimensionless (normalized) gas uptake term for comparison purpose. Assuming all particles perform similarly in the reactor, particles number has no role in the dimensionless gas uptake defined as the amount of $CO_2$ consumed at any time over the overall $CO_2$ consumed over process course. The normalization was conducted as the gas uptake and any time divided by gas uptake at the end of the test. This approach will eliminate the role of the number of particles. As shown in Fig. 2(B), the modeling result for gas consumption reveals a two-stage process that is similar to that observed experimentally. Moreover, the gas uptake history is in a good agreement with the experimentally measured values.

Furthermore, Lederhos et al. (Lederhos et al., 1996) conducted an experimental study in a batch reactor to investigate the effects of the kinetic inhibitors on hydrate inhibition, as evaluated by measuring the gas consumption versus time. The process history graph clearly shows the hydrate nucleation and growth processes that are captured in the current model. They schematically illustrated the nucleation stage (or induction time) as the time elapsed before the first detectable gas consumption (growth stage). Yin et al. reported a similar gas uptake trend for $CH_4$ hydrate formation in a batch stirred reactor based on the results of Englezos et al.

(Englezos et al., 1987; Yin et al., 2018). They considered the first stage as the gas dissolution and induction period, and at this stage, the amount of gas consumption is very small due to the dissolution of the gas molecules in the liquid phase. These practical observations corroborate the presented multi-stage model as a consistent paradigm for the hydration process. He et al. investigated the nucleation of the $CO_2$ hydrate using molecular simulation, and a small $CO_2$ mass fraction during the nucleation stage was observed (He et al., 2017). The same trend in the results using molecular simulation was reported by Bi et al. (Bi et al., 2016) Jacobson et al. simulated the mechanism of the nucleation process using molecular simulation by showing the number of occupied cages versus time. They showed that at the nucleation stage, the cages are not occupied by the $CO_2$ molecules, and as hydrate growth starts, the cages are occupied by the $CO_2$ molecules (Jacobson et al., 2010b). All of these studies support the history trends presented in Fig. 2, confirming the validity of the modeling framework.

## 4. Non-isothermal behavior

To capture the thermal history of the reacting particles, integration of the heat transfer and kinetics of gas hydrate formation was implemented. Accordingly, energy conservation and constitutive equations were added to the primary multi-stage model and solved simultaneously (Table 2). The particle temperature profile resulting from the thermal profiles of the individual stages is presented in Fig. 3. Regarding the gas hydration temperature profile, an initial rise followed by a decline and final settling at approximately 273.5 K for the $CO_2$ hydration case has been reported in many experimental studies. This profile can be explained based on the release of heat due to the initial nucleation and hydration. Sloan and Koh highlighted that the rapid increase in temperature indicates hydrate formation in a high-pressure cell with constant volume (Sloan and Koh, 2008). The temperature of the cell/particle subsequently gradually decreases due to nucleation rate mitigation and heat transfer to the surrounding particles. The temperature settlement at the final value can be observed in Stage 3, as shown by theoretical (this work) results. The thermal capability is an applied added value of the current model that has not been taken into account in previous models (Bollavaram et al., 2000; Shi et al., 2011). While the proposed model importantly allows the prediction of the thermal trends of the particle and the reactor, parameter tuning must be conducted for any specific case study using the experimental data under relevant conditions. The model-based temperature profile, Fig. 3, well simulates the temperature history trends observed in the experimental works including the temperature peak and settlement.

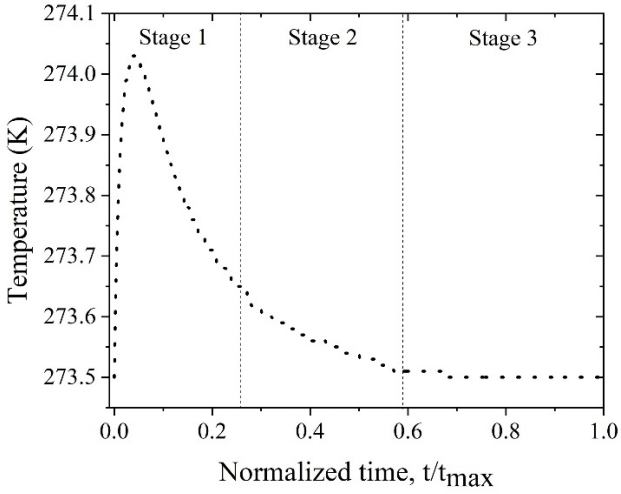


Fig. 3. Temperature profile of the $CO_2$ hydration process comprising three stages of the thermal history achieved via MSSCM simulating experimentally seen temperature peak and settlement.

## 5. Model analysis

### 5.1. Sensitivity analysis of the reaction constant rates

Several studies have investigated the $CO_2$ hydration reaction rate during gas hydrate formation (Bergeron and Servio, 2008; Chun and Lee, 1996; Malegaonkar et al., 1997; Ou et al., 2016; Verrett and Servio, 2016). A sensitivity analysis of the competing reactions using the rates constants $k_2$ and $k_3$ was carried out to investigate the species distribution and steps/phases lifetime and induction time.

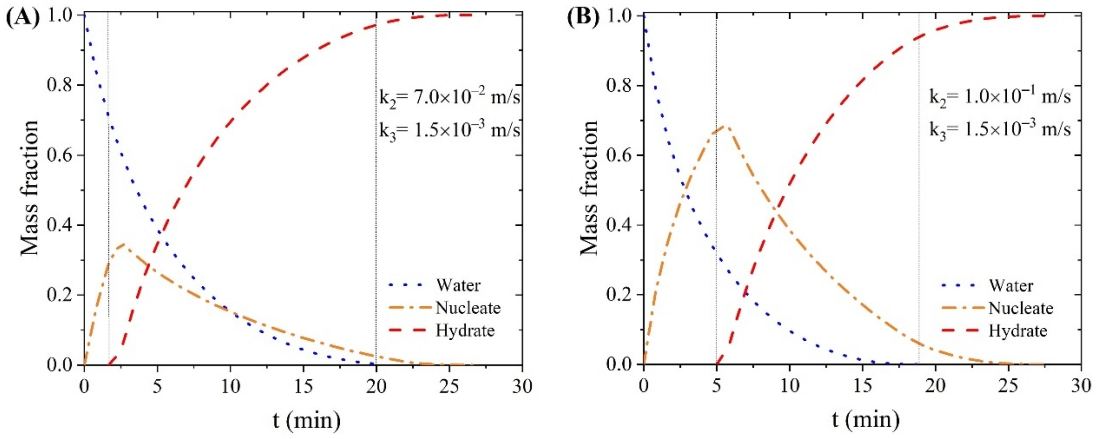

Fig. 4. Results of the multi-stage nucleation and growth model for the mass fractions of water, nucleate and hydrate versus time for (A) $k_2$=7.0×10$^{-2}$ m/s and (B) $k_2$=1.0×10$^{-1}$ m/s. The black dotted lines separate the three stages in MSSCM.

Fig. 4 indicates the phases' distributions inside the particle, the duration of the individual stages and the whole process for the two nucleation rate constants ($k_2$) and the hydration rate constant $k_3$ = 1.5×10$^{-3}$ m/s. The faster nucleation process results in higher nucleate accumulation inside the particle, and the nucleate shows a stronger peak by $k_2$, whereas the hydration rate is slow and controlling. A greater amount of $CO_2$ penetrating into the water droplet would be consumed for the nucleation process, resulting in a longer induction time due to the lack of $CO_2$ for growth. This behavior is consistent with the mathematical estimation of the induction time in which the $CO_2$ profiles in Stage 1 and 2 play a crucial role. A delay in hydration process initiation leads to a longer process completion time, i.e., from 26.6 min for $k_2$ = 1.0×10$^{-1}$ m/s to 28.4 min for $k_2$ = 7.0×10$^{-2}$ m/s. The induction time increases, and the nucleate shows a stronger peak by $k_2$. For small $k_2$ values, the $CO_2$ capture process proceeds mainly through Stage 2 (lasting for 18 min, ~67% of the overall time), in which all three phases exist, while for $k_2$ = 1.0×10$^{-1}$ m/s, Stage 2 lasts for 12.5 min, ~44% of the overall time.

In the second sensitivity analysis, the effects of varying $k_3$ were examined while $k_2$ was considered to be a constant parameter in MSSCM for comparison. Fig. 5 illustrates the results for $k_3$ = 1.3×10$^{-3}$ m/s and $k_3$ = 1.5×10$^{-3}$ m/s at $k_2$ = 9.0×10$^{-2}$ m/s. As shown in Fig. 5, as the $k_3$ value increases, the time required for total depletion of the nucleate core decreases, which results in higher impacts on Stages 2 and 3 compared to Stage 1. The induction is shorter at higher $k_3$ values, and the process period mainly consists of Stages 2 and 3. Combining both individual analyses, it can be concluded that the $k_2$×$k_3$ is a reasonable measure for explaining the process behavior. A smaller $k_2$×$k_3$ would lead to a longer induction time, larger nucleate fraction peak, and longer completion time.

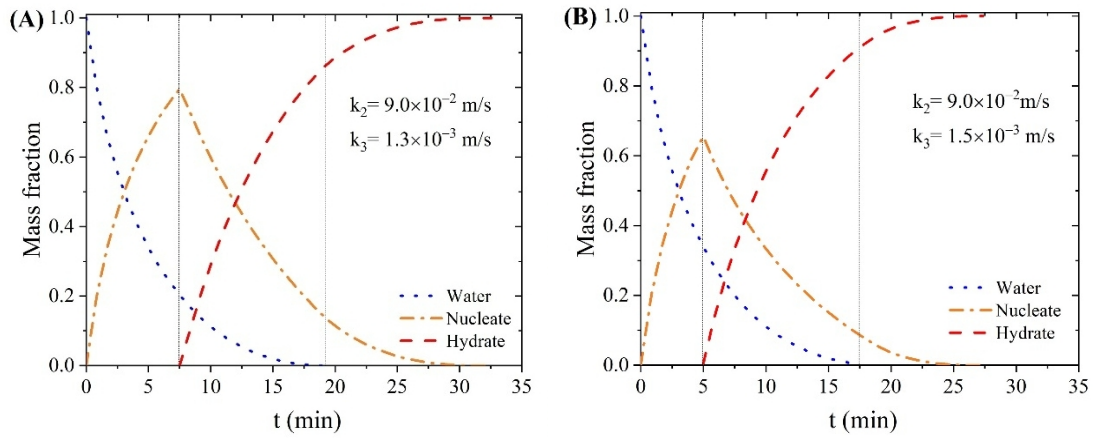


Fig. 5. Results of the multi-stage nucleation and growth model for the mass fractions of water, nucleate and hydrate versus time for (A) $k_3$=1.3×10$^{-3}$ m/s and (B) $k_3$=1.5×10$^{-3}$ m/s. The black dotted lines separate the stages in MSSCM.

## 5.2. Effects of the $CO_2$ solubility in MSSCM

An analysis of the effects of the solubility on the $CO_2$ consumed using the experimental $CO_2$ solubility in water at 3.25 MPa and 270 K (Diamond and Akinfiev, 2003) has been investigated in this study. $CO_2$ dissolution in water under 3.25 MPa and 270 K is approximately 0.0325 mole $CO_2$ / mole $H_2O$ (Diamond and Akinfiev, 2003), which is not enough to fully form the hydrate ($CO_2 \cdot 5.75H_2O$) or even nucleate ($CO_2 \cdot mH_2O$, m > 5.75). For hydrate formation, a solid solution of 0.174 (mole $CO_2$ / mole $H_2O$) must be achieved. Accordingly, it was assumed that the $CO_2$ needed for this process is mainly provided externally through diffusion. Fig. 6 illustrated the effects of the $CO_2$ solubility on the $CO_2$ consumption in MSSCM. It can be seen from Fig. 6 that the $CO_2$ solubility does not have significant effects on the amount of $CO_2$ consumption during $CO_2$ hydrate nucleation and growth.

The $CO_2$ solubility in water may raise concerns about the applicability of SCM for the current case study. Since the $CO_2$ diffusion rate decreases drastically upon formation of the hydrate layer, the overall process is controlled by the $CO_2$ mass transfer rate, which allows a minor amount of $CO_2$ to reach the interior and, in particular, the central parts of the water droplet. This behavior reasonably justifies the applicability of SCM, as demonstrated by its successful use in the literature (Falenty et al., 2013; Henning et al., 2000; Staykova et al., 2003). For the gas uptake underestimation, one may combine the gas consumed through the dissolution and nucleation mechanisms. In other words, the gas consumed for nucleation might be fitted to be representative of both dissolution and nucleation gas consumption, where individual portions

can be estimated through thermodynamic estimations. Given the significantly higher gas consumption in the growth stage compared to the dissolution and nucleation stages, this simplification would not result in significant errors as shown in Fig. 6.

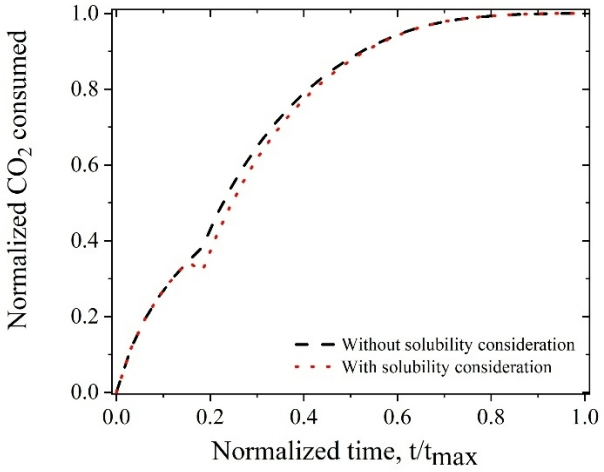


Fig. 6. Effects of the $CO_2$ solubility on the $CO_2$ consumption estimated in MSSCM

## 5.3. Internal $CO_2$ concentration

As a mass transfer-controlled process, the intensification and control of $CO_2$ hydration might benefit significantly from insights on the distributed and time-dependent concentration profiles inside the reacting element. The proposed model readily offers such insightful data, in contrast to the challenges in achieving such data from practical measurements. The concentration difference across the phases' layers ($\Delta C/\Delta r$) was estimated for the hydrate, $(C^{b}_{CO_2} - C^{N,H}_{CO_2})/(R_p - r_2)$, and nucleate, $(C^{N,H}_{CO_2} - C^{W,N}_{CO_2})/(r_2 - r_1)$, layers during Stage 2 as presented in Figure 7. Water conversion, as an indicator of reaction progress, is also depicted. The concentration gradient across the nucleate layer is higher than that in the hydrate layer at any time during the second stage.

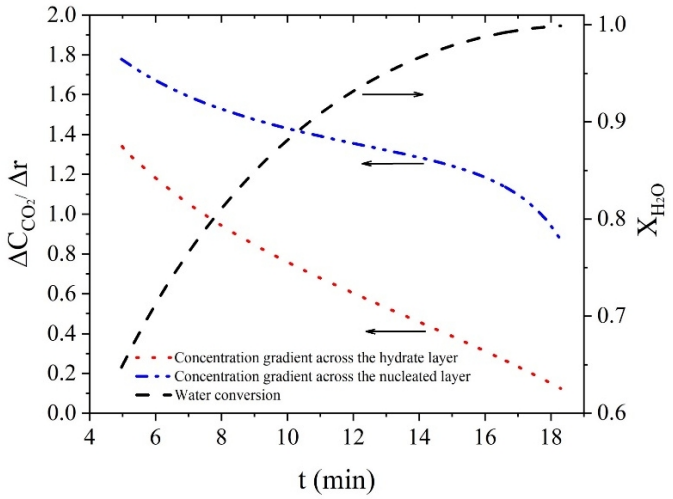


Fig. 7. Concentration difference across the hydrate and nucleate layers and water conversion profile in Stage 2.

As the diffusivity ($D_e$) is supposed to be higher in the nucleate than in the hydrate, mass transfer in the hydrate is predominant in controlling the conversion rate compared to the nucleate. However, the share of the nucleate that is mass transfer resistant cannot be ignored. From this viewpoint, a detailed quantitative evaluation of each phase share is feasible through MSSCM.

### 5.4. Model-based nucleate structure identification

The nucleate configuration can be presented as $CO_2.mH_2O$ with a considerable uncertainty associated with the nucleation number value, *m,* in contrast to the hydration number, *n,* for which we use a value of 5.75 from the literature (Sun and Kang, 2016). Different nucleation numbers ($m$=7, 10, 15, 20) were tested in this analysis. As shown in Fig. 8, the proposed model provides a tool to explain different gas uptake profiles observed in practice based on the possible differences between the hydration and nucleation numbers and hence the variations in physical properties. For $m>>n$, the induction time and the nucleation stages are expected to be more distinguishable in the gas uptake profile. For $m\sim n$, the nucleation and hydration stages behave similarly in the gas consumption history, thus requiring the use of the phase distribution profiles to detect the stages and the induction time. Since all of the profile trends shown in Fig. 8 have been observed in practical experiments, the proposed model provides judgment criteria for assessing how the formed-nucleate structure deviates from the hydrate structure under the experimental condition of interest.

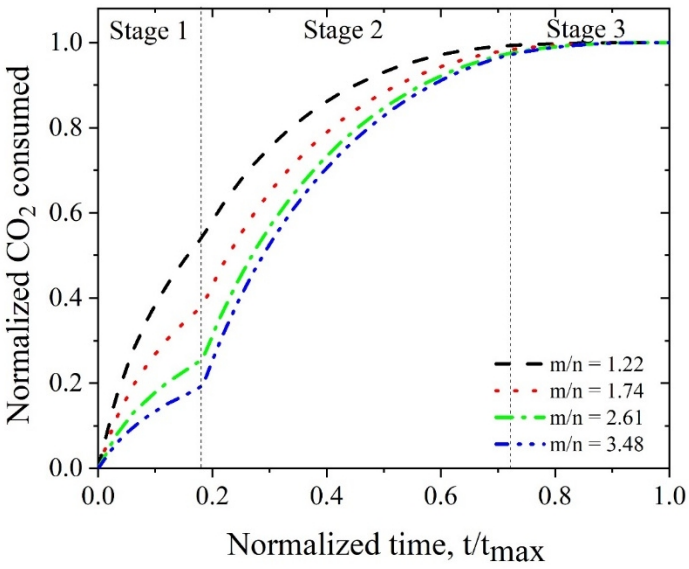


Fig. 8. Model-based gas uptake profile for different nucleation numbers. All types of the trends shown have been observed in the experimental literature, thus indicating the diversity of possible nucleation numbers.

## 6. Conclusions

A multi-stage-multi-reaction modeling framework was proposed and successfully used for the $CO_2$ hydration case. Although this paper focuses on $CO_2$ hydrate formation, the concept is generic enough to be applied to other hydration processes, such as $CH_4$ hydration, with minor changes. Moreover, the model was presented for a spherical geometry but can potentially be adapted for other geometrical domains, such as slab and cylindrical geometries, depending on the reactor, pipeline, hydrodynamics regime, etc. The proposed model was capable of not only capturing the $CO_2$ hydration progress but also predicting nucleate phase formation and depletion. The former, in particular, is of crucial importance and enables a numerical estimation of the induction time. The induction time has been frequently observed in experimental tests. However, this study is the first to propose a model-based estimation method to predict the nucleation stage. Moreover, the model's capability in capturing the dynamic thermal behavior of the $CO_2$ hydration reaction was demonstrated. Based on the temperature profile, the hydration start time and progress pattern are detectable. A model-based criterion was proposed to use the experimentally measured gas uptake profiles to estimate the nucleation number, i.e., $m$ in $CO_2 \cdot mH_2O$. The numerical estimation of the internal concentration profiles for a hydrating particle was demonstrated. The presented model requires a minor computation time (less than a minute) using MATLAB for a single particle simulation and thus is

computationally suitable for use at the reactor scale, in which enormous particles are present. The present study, therefore, provides a foundation for future research towards enhancing our understanding of gas nucleation and hydration process behavior based on predictive models at various spatiotemporal scales.

## Nomenclature

| | |
|---|---|
| $C_{CO_2}$ | $CO_2$ concertation inside the particle ($mol/m^3$) |
| $C_{CO_2}^b$ | concentration of $CO_2$ in gas bulk ($mol/m^3$) |
| $C_{CO_2}^{W,H}$ | $CO_2$ concentration at the water/hydrate interface ($mol/m^3$) |
| $C_{CO_2}^{W,N}$ | $CO_2$ concentration at the water/nucleate interface ($mol/m^3$) |
| $CO_2$ | carbon dioxide |
| $C_{p,1}$ | specific heat capacity in Stage 1 ($kJ/kgK$) |
| $C_{p,2}$ | specific heat capacity in Stage 2 ($kJ/kgK$) |
| $C_{p,3}$ | specific heat capacity in Stage 3 ($kJ/kgK$) |
| $D_e$ | effective $CO_2$ diffusivity coefficient ($m^2/s$) |
| $D_{e,1}$ | effective $CO_2$ diffusivity coefficient in Stage 1 ($m^2/s$) |
| $D_{e,2}$ | effective $CO_2$ diffusivity coefficient in Stage 2 ($m^2/s$) |
| $D_{e,3}$ | effective $CO_2$ diffusivity coefficient in Stage 3 ($m^2/s$) |
| $h$ | heat transfer coefficient ($kW/m^2K$) |
| $H_2O$ | water |
| $k_2$ | reaction rate constant for Eq. (1) ($m/s$) |
| $k_3$ | reaction rate constant for Eq. (2) ($m/s$) |
| m | nucleation number |
| $MW_{avg,2}$ | average molecular weight in Stage 2 ($g/mol$) |
| $MW_{avg,3}$ | average molecular weight in Stage 3 ($g/mol$) |
| $MW_{H_2O}$ | molecular weight of water ($g/mol$) |
| $MW_N$ | molecular weight of nucleate ($g/mol$) |
| n | hydration number |
| m | nucleation number |
| $r$ | radius ($m$) |
| $r_1, r^{W.N}$ | radius at water/nucleate interface ($m$) |
| $r_2, r^{N.H}$ | radius at nucleate/hydrate interface ($m$) |

| | | |
|---|---|---|
| $r_h$ | rate of water conversion to hydrate ($kg/m^2s$) |
| $r_N$ | rate of nucleate conversion to hydrate ($kg/m^2s$) |
| $r_W$ | rate of the water conversion to nucleate ($kg/m^2s$) |
| $R_p$ | particle radius ($m$) |
| $t$ | time (min) |
| $t_0$ | initial time (min) |
| $t_1$ | time when hydrate growth starts (min) |
| $t_2$ | time when fresh water is fully consumed (min) |
| $t_3$ | time when nucleate is fully consumed (min) |
| $T$ | temperature (K) |
| $T_1$ | temperature at water/nucleate interface (K) |
| $T_2$ | temperature at nucleate/hydrate interface (K) |
| $T_b$ | temperature at bulk gas (K) |
| $X_{H_2O}$ | water conversion |

**Greek Letters**

| | |
|---|---|
| $\rho$ | density ($kg/m^3$) |
| $\rho_{avg,2}$ | average density at Stage 2 ($kg/m^3$) |
| $\rho_{avg,3}$ | average density at Stage 3 ($kg/m^3$) |
| $\rho_N$ | density of nucleate ($kg/m^3$) |
| $\vartheta_1, \vartheta_2$ | stoichiometry coefficient ratios |
| $\Delta H_2$ | reaction enthalpy in Eq. (2) ($kJ/kg$) |
| $\Delta H_3$ | reaction enthalpy in Eq. (3) ($kJ/kg$) |

**Sub-/Superscripts**

| | |
|---|---|
| $b$ | gas bulk |
| $CO_2$ | carbon dioxide |
| $g$ | gaseous phase |
| $H$ | hydrate |
| $H_2O$ | water |
| $N$ | nucleate |
| $N.H$ | nucleate/hydrate interface |
| $p$ | particle |

| | | |
|---|---|---|
| $s$ | solid phase |
| $W$ | water |
| $W.N$ | water/nucleate interface |

## Appendix: Model derivation

### Stage 1:

The $CO_2$ molar rate due to the reaction in the nucleate-hydrate interface is:

$$M_{r,1} = 4\pi {r_1}^2 \vartheta_1 k_2 C_{CO_2}^{W,N} \quad (A.1)$$

in which $M_{r,1}$ is the $CO_2$ molar reaction rate at Stage 1. Using Fick's law, the rate of the $CO_2$ diffusion is given by:

$$M_{d,1} = 4\pi r^2 D_{e,1} \frac{dC_{CO_2}^{W,N}}{dr} \quad (A.2)$$

where $M_{d,1}$ is the $CO_2$ diffusion rate at Stage 1. Integrating from $r_1$ to $R_p$ and $C_{CO_2}^{W,N}$ to $C_{CO_2}^{b}$:

$$M_{d,1} \int_{r_1}^{R_p} \frac{1}{r^2}\, dr = -4\pi D_{e,1} \int_{C_{CO_2}^{W,N}}^{C_{CO_2}^{b}} dC_{CO_2} \quad (A.3)$$

or

$$M_{d,1}\left(\frac{1}{R_p} - \frac{1}{r_1}\right) = 4\pi D_{e,1}\left(C_{CO_2}^{b} - C_{CO_2}^{W,N}\right) \quad (A.4)$$

or

$$M_{d,1} = 4\pi D_{e,1} \frac{\left(C_{CO_2}^{b} - C_{CO_2}^{W,N}\right)}{\frac{1}{r_1} - \frac{1}{R_p}} \quad (A.5)$$

Diffusion of $CO_2$ through the nucleate layer is equal to the $CO_2$ reaction in the water/nucleate interface:

$$M_{r,1} = M_{d,1} \quad (A.6)$$

or

$$4\pi {r_1}^2 \vartheta_1 k_2 C_{CO_2}^{W,N} = 4\pi D_{e,1} \frac{\left(C_{CO_2}^{b} - C_{CO_2}^{W,N}\right)}{\frac{1}{r_1} - \frac{1}{R_p}} \quad (A.7)$$

or

$$C_{CO_2}^{b} - C_{CO_2}^{W,N} - \frac{r_1^{\,2}\vartheta_1 k_2 C_{CO_2}^{W,N}\left(\frac{1}{r_1}-\frac{1}{R_p}\right)}{D_{e,1}} = 0 \qquad (A.8)$$

or

$$C_{CO_2}^{b} - C_{CO_2}^{W,N}\left(1 + \frac{r_1^{\,2}\vartheta_1 k_2\left(\frac{1}{r_1}-\frac{1}{R_p}\right)}{D_{e,1}}\right) = 0 \qquad (A.9)$$

or

$$1 - \frac{C_{CO_2}^{W,N}}{C_{CO_2}^{b}}\left(1 + \frac{r_1^{\,2}\vartheta_1 k_2\left(\frac{1}{r_1}-\frac{1}{R_p}\right)}{D_{e,1}}\right) = 0 \qquad (A.10)$$

or

$$1 - \frac{C_{CO_2}^{W,N}}{C_{CO_2}^{b}}\left(1 + \frac{\vartheta_1 k_2 R_p}{D_{e,1}}\left(\frac{r_1}{R_p}\right)^2\left(\frac{1}{\left(\frac{r_1}{R_p}\right)}-1\right)\right) = 0 \qquad (A.11)$$

Water consumption rate is given by:

$$N_{H_2O} = -\frac{d}{dt}\left(\frac{4\pi r_1^3 \rho_{H_2O}}{3\,MW_{H_2O}}\right) \qquad (A.12)$$

in which $N_{H_2O}$ is the water consumption rate. The relation between the water conversion and molar rate due to the reaction is:

$$N_{H_2O} = \frac{1}{\vartheta_1} M_{r,1} \qquad (A.13)$$

Combining eq (A12 and A13) results in:

$$\frac{dr_1}{dt} = -\frac{MW_{H_2O}}{\rho_{H_2O}} k_2 C_{CO_2}^{W,N} \qquad (A.14)$$

**Non-isothermal equations in Stage 1:**

Non-isothermal equations are based on the energy balance around the particle at each stage:

$$\frac{4\pi R_p^3 \rho_{H_2O}}{3\,MW_{H_2O}} C_{p,1}\frac{dT}{dt} = 4\pi R_p^2 h(T_b - T) - 4\pi r_1^2 k_2 C_{CO_2}^{W,N}\Delta H_2 \qquad (A.15)$$

or

$$\frac{dT}{dt} = \frac{h(T_b - T) - \left(\frac{r_1}{R_p}\right)^2 k_2 \Delta H_2 C_{CO_2}^{W,N}}{\frac{R_p \rho_{H_2O}}{3MW_{H_2O}} C_{p,1}} \quad (A.16)$$

**Stage 2:**

$CO_2$ reaction rate at the water-nucleate interface is:

$$M_{r,2} = 4\pi r_1^2 \vartheta_1 k_2 C_{CO_2}^{W,N} \quad (A.17)$$

where $M_{r,2}$ is the $CO_2$ reaction rate at the water-nucleate interface at Stage 2. $CO_2$ diffusion rate at the water-nucleate interface is given by:

$$M_{d,2} = -4\pi r_1^2 D_{e,2} \frac{dC_{CO_2}^{W,N}}{dr} \quad (A.18)$$

in which $M_{d,2}$ is the $CO_2$ diffusion rate between the water-nucleate interface and nucleate-hydrate interface at Stage 2. Or:

$$M_{d,2} = 4\pi D_{e,2} \frac{(C_{CO_2}^{N,H} - C_{CO_2}^{W,N})}{\frac{1}{r_1} - \frac{1}{r_2}} \quad (A.19)$$

$CO_2$ diffusion rate is equal to $CO_2$ reaction rate:

$$M_{r,2} = M_{d,2} \quad (A.20)$$

or

$$C_{CO_2}^{N,H} - C_{CO_2}^{W,N} - \frac{r_1^2 \vartheta_1 k_2 C_{CO_2}^{W,N}}{D_{e,2}} \left(\frac{1}{r_1} - \frac{1}{r_2}\right) \quad (A.21)$$

or

$$\frac{C_{CO_2}^{N,H}}{C_{CO_2}^{b}} - \frac{C_{CO_2}^{W,N}}{C_{CO_2}^{b}} \left(1 + \frac{\vartheta_1 k_2 R_p}{D_{e,2}} \left(\frac{r_1}{R_p}\right)^2 \left(\frac{1}{\left(\frac{r_1}{R_p}\right)} - \frac{1}{\left(\frac{r_2}{R_p}\right)}\right)\right) = 0 \quad (A.22)$$

Water consumtion is given by:

$$N'_{H_2O} = -\frac{d}{dt}\left(\frac{4\pi r_1^3 \rho_{H_2O}}{3\,MW_{H_2O}}\right) \quad (A.23)$$

in which $N'_{H_2O}$ is water consumption at Stage 2. The relation between the water conversion and molar rate due to the reaction is:

$$N'_{H_2O} = \frac{1}{\vartheta_1} M_{r,2} \quad \text{(A.24)}$$

or

$$\frac{dr_1}{dt} = -\frac{MW_{H_2O}}{\rho_{H_2O}} k_2 C^{W,N}_{CO_2} \quad \text{(A.25)}$$

$CO_2$ Diffusion rate through the nucleate layer is given by:

$$M'_{d,2} = 4\pi D_{e,2} \frac{\left(C^{b}_{CO_2} - C^{N,H}_{CO_2}\right)}{\frac{1}{r_2} - \frac{1}{R_p}} \quad \text{(A.26)}$$

where $M'_{d,2}$ is the $CO_2$ diffusion rate between bulk $CO_2$ and nucleate-hydrate layer. $CO_2$ reaction rate at the nucleate-hydrate interface is:

$$M_N = 4\pi r_2^2 \vartheta_2 k_3 C^{N,H}_{CO_2} \quad \text{(A.27)}$$

in which $M_N$ is the $CO_2$ reaction rate at the nucleate-hydrate interface. Mass balance around the particle at Stage 2 is:

$$M'_{d,2} = M_{r,2} + M_N \quad \text{(A.28)}$$

or

$$C^{b}_{CO_2} - C^{N,H}_{CO_2} - \frac{{r_1}^2 \vartheta_1 k_2 C^{W,N}_{CO_2} + r_2^2 \vartheta_2 k_3 C^{N,H}_{CO_2}}{D_{e,2}} \left(\frac{1}{r_2} - \frac{1}{R_p}\right) = 0 \quad \text{(A.29)}$$

or

$$1 - \frac{C^{N,H}_{CO_2}}{C^{b}_{CO_2}} - \left(\frac{\vartheta_1 k_2 R_p C^{W,N}_{CO_2}}{D_{e,2}\ C^{b}_{CO_2}} \left(\frac{r_1}{R_p}\right)^2 + \frac{\vartheta_2 k_3 R_p C^{N,H}_{CO_2}}{D_{e,2}\ C^{b}_{CO_2}} \left(\frac{r_2}{R_p}\right)^2\right) \left(\frac{1}{\left(\frac{r_2}{R_p}\right)} - 1\right) = 0 \quad \text{(A.30)}$$

The rate of nucleate consumption is given by:

$$N_N = -\frac{d}{dt}\left(\frac{4\pi r_2^3 \rho_N}{3\, MW_N}\right) \quad \text{(A.31)}$$

in which $N_N$ is the rate of nucleate consumption. The relation between the rate of nucleate consumption and reaction at the nucleate-hydrate interface is:

$$N_N = \frac{1}{\vartheta_2} M_N \quad \text{(A.32)}$$

or

$$\frac{dr_2}{dt} = -\frac{MW_N}{\rho_N} k_3 C^b_{CO_2} \frac{C^{N,H}_{CO_2}}{C^b_{CO_2}} \quad (A.33)$$

**Non-isothermal equations in Stage 2:**

An energy balance around the particle at Stage 2 is given by:

$$\frac{4\pi R_p^3 \rho_{avg,2}}{3\, MW_{avg,2}} C_{p,2} \frac{dT}{dt} = 4\pi R_p^2 h(T_b - T) - 4\pi r_1^2 k_2 C^{W,N}_{CO_2} \Delta H_2 - 4\pi r_2^2 k_3 C^{N,H}_{CO_2} \Delta H_3 \quad (A.34)$$

or

$$\frac{dT}{dt} = \frac{h(T_b - T) - \left(\frac{r_1}{R_p}\right)^2 k_2 \Delta H_2 C^{W,N}_{CO_2} - \left(\frac{r_2}{R_p}\right)^2 k_3 \Delta H_3 C^{N,H}_{CO_2}}{\frac{R\rho_{avg,2}}{3MW_{avg,2}} C_{p,2}} \quad (A.35)$$

**Stage 3:**

$CO_2$ reaction rate at the nucleate-hydrate interface is:

$$M_{r,3} = 4\pi {r_2}^2 \vartheta_2 k_3 C^{N,H}_{CO_2} \quad (A.36)$$

where $M_{r,3}$ is the $CO_2$ reaction rate at the nucleate-hydrate interface at Stage 3. $CO_2$ diffusion rate at Stage 3 is given by:

$$M_{d,3} = 4\pi D_{e,3} \frac{(C^b_{CO_2} - C^{N,H}_{CO_2})}{\frac{1}{r_2} - \frac{1}{R_p}} \quad (A.37)$$

in which $M_{d,3}$ is the $CO_2$ diffusion rate between bulk $CO_2$ and nucleate-hydrate interface. $CO_2$ rate of the reaction is equal to the rate of the diffusion:

$$M_{r,3} = M_{d,3} \quad (A.38)$$

or

$$C^b_{CO_2} - C^{N,H}_{CO_2} - \frac{{r_2}^2 \vartheta_2 k_3 C^{W,N}_{CO_2} \left(\frac{1}{r_2} - \frac{1}{R_p}\right)}{D_{e,3}} = 0 \quad (A.39)$$

or

$$1 - \frac{C^{N,H}_{CO_2}}{C^b_{CO_2}} \left(1 + \frac{\vartheta_2 k_3 R_p}{D_{e,3}} \left(\frac{r_2}{R_p}\right)^2 \left(\frac{1}{\left(\frac{r_2}{R_p}\right)} - 1\right)\right) = 0 \quad (A.40)$$

The rate of nucleate consumption is given by:

$$N_N^{'} = -\frac{d}{dt}\left(\frac{4\pi r_2^3 \rho_N}{3\,MW_N}\right) \quad (A.41)$$

where $N_N^{'}$ is the rate of nucleate consumption at Stage 3. The relation between nucleate consumption and reaction rate in Stage 3 is:

$$N_N^{'} = \frac{1}{\vartheta_2} M_{r,3} \quad (A.42)$$

or

$$\frac{dr_2}{dt} = -\frac{MW_N}{\rho_N} k_3 C_{CO_2}^{b} \frac{C_{CO_2}^{N,H}}{C_{CO_2}^{b}} \quad (A.43)$$

## Non-isothermal equations in Stage 3:

An energy balance around the particle at stage 3 is given by:

$$\frac{4\pi R_p^3 \rho_{avg,3}}{3\,MW_{avg,3}} C_{p,3} \frac{dT}{dt} = 4\pi R_p^2 h(T_b - T) - 4\pi r_2^2 k_3 C_{CO_2}^{N,H} \Delta H_2 \quad (A.44)$$

or

$$\frac{dT}{dt} = \frac{h(T_b - T) - \left(\frac{r_2}{R_p}\right)^2 k_3 \Delta H_3 C_{CO_2}^{N,H}}{\frac{R_p \rho_{avg,3}}{3MW_{avg,3}} C_{p,3}} \quad (A.45)$$

# References


Amiri, A., Bekker, A.V., Ingram, G.D., Livk, I., Maynard, N.E., 2013a. A 1-D non-isothermal dynamic model for the thermal decomposition of a gibbsite particle. Chemical Engineering Research and Design 91(3), 485-496.

Amiri, A., Ingram, G.D., Bekker, A.V., Livk, I., Maynard, N.E., 2013b. A multi-stage, multi-reaction shrinking core model for self-inhibiting gas–solid reactions. Advanced Powder Technology 24(4), 728-736.

Amiri, A., Ingram, G.D., Maynard, N.E., Livk, I., Bekker, A.V., 2015. An unreacted shrinking core model for calcination and similar solid-to-gas reactions. Chemical Engineering Communications 202(9), 1161-1175.

Bai, D., Chen, G., Zhang, X., Wang, W., 2011. Microsecond molecular dynamics simulations of the kinetic pathways of gas hydrate formation from solid surfaces. Langmuir 27(10), 5961-5967.

Bai, D., Chen, G., Zhang, X., Wang, W., 2012. Nucleation of the $CO_2$ hydrate from three-phase contact lines. Langmuir 28(20), 7730-7736.

Bergeron, S., Servio, P., 2008. Reaction rate constant of $CO_2$ hydrate formation and verification of old premises pertaining to hydrate growth kinetics. AIChE Journal 54(11), 2964-2970.

Bi, Y., Porras, A., Li, T., 2016. Free energy landscape and molecular pathways of gas hydrate nucleation. J Chem Phys 145(21), 211909.

Bollavaram, P., Devarakonda, S., Selim, M.S., Sloan, E.D., 2000. Growth kinetics of single crystal sII hydrates: Elimination of mass and heat transfer effects. Annals of the New York Academy of Sciences 912(1), 533-543.

Chun, M.-K., Lee, H., 1996. Kinetics of formation of carbon dioxide clathrate hydrates. Korean Journal of Chemical Engineering 13(6), 620-626.

Clarke, M.A., Bishnoi, P.R., 2005. Determination of the intrinsic kinetics of of $CO_2$ gas hydrate decomposition using in-situ particle size analysis. Chemical Engineering Science 60(3), 695-709.

Dashti, H., Lou, X., 2018. Gas hydrate-based $CO_2$ separation process: Quantitative assessment of the effectiveness of various chemical additives involved in the process. Springer International Publishing, Cham, pp. 3-16.

Dashti, H., Thomas, D., Amiri, A., Lou, X., 2019. Variations of the shrinking core model for effective kinetics modeling of the gas hydrate-based $CO_2$ capture process in: Kiss, A., Zondervan, E., Lakerveld, R., Özkan, L. (Eds.), Computer Aided Chemical Engineering. Elsevier p. 2030.

Dashti, H., Zhehao Yew, L., Lou, X., 2015. Recent advances in gas hydrate-based $CO_2$ capture. Journal of Natural Gas Science and Engineering 23, 195-207.

Diamond, L.W., Akinfiev, N.N., 2003. Solubility of $CO_2$ in water from −1.5 to 100 °C and from 0.1 to 100 MPa: evaluation of literature data and thermodynamic modelling. Fluid Phase Equilibria 208(1), 265-290.

Englezos, P., 1993. Clathrate hydrates. Industrial & Engineering Chemistry Research 32(7), 1251-1274.

Englezos, P., Kalogerakis, N., Dholabhai, P.D., Bishnoi, P.R., 1987. Kinetics of formation of methane and ethane gas hydrates. Chemical Engineering Science 42(11), 2647-2658.

English, N.J., MacElroy, J.M.D., 2015. Perspectives on molecular simulation of clathrate hydrates: Progress, prospects and challenges. Chemical Engineering Science 121, 133-156.

Eslamimanesh, A., Mohammadi, A.H., Richon, D., Naidoo, P., Ramjugernath, D., 2012. Application of gas hydrate formation in separation processes: A review of experimental studies. The Journal of Chemical Thermodynamics 46, 62-71.

Falenty, A., Salamatin, A.N., Kuhs, W.F., 2013. Kinetics of $CO_2$-hydrate formation from ice powders: Data summary and modeling extended to low temperatures. The Journal of Physical Chemistry C 117(16), 8443-8457.

Hashemi, S., Macchi, A., Servio, P., 2007. Gas hydrate growth model in a semibatch stirred tank reactor. Industrial & Engineering Chemistry Research 46(18), 5907-5912.

He, Z., Linga, P., Jiang, J., 2017. What are the key factors governing the nucleation of $CO_2$ hydrate? Phys Chem Chem Phys 19(24), 15657-15661.

Henning, R.W., Schultz, A.J., Thieu, V., Halpern, Y., 2000. Neutron diffraction studies of $CO_2$ clathrate hydrate: Formation from deuterated ice. The Journal of Physical Chemistry A 104(21), 5066-5071.

Jacobson, L.C., Hujo, W., Molinero, V., 2010a. Amorphous precursors in the nucleation of clathrate hydrates. Journal of the American Chemical Society 132(33), 11806-11811.

Jacobson, L.C., Hujo, W., Molinero, V., 2010b. Nucleation pathways of clathrate hydrates: Effect of guest size and solubility. The Journal of Physical Chemistry B 114(43), 13796-13807.

Khurana, M., Yin, Z., Linga, P., 2017. A review of clathrate hydrate nucleation. ACS Sustainable Chemistry & Engineering.

Kvamme, B., Graue, A., Aspenes, E., Kuznetsova, T., Granasy, L., Toth, G., Pusztai, T., Tegze, G., 2004. Kinetics of solid hydrate formation by carbon dioxide: Phase field theory of hydrate nucleation and magnetic resonance imaging. Physical Chemistry Chemical Physics 6(9), 2327-2334.

Lederhos, J.P., Long, J.P., Sum, A., Christiansen, R.L., Sloan, E.D., 1996. Effective kinetic inhibitors for natural gas hydrates. Chemical Engineering Science 51(8), 1221-1229.

Liang, S., Liang, D., Wu, N., Yi, L., Hu, G., 2016. Molecular Mechanisms of Gas Diffusion in $CO_2$ Hydrates. The Journal of Physical Chemistry C 120(30), 16298-16304.

Linga, P., Kumar, R., Englezos, P., 2007. Gas hydrate formation from hydrogen/carbon dioxide and nitrogen/carbon dioxide gas mixtures. Chemical Engineering Science 62(16), 4268-4276.

Lirio, C., Pessoa, F., 2013. Enthalpy of dissociation of simple and mixed carbon dioxide clathrate hydrate. Chemical Engineering Transactions 32.
Malegaonkar, M.B., Dholabhai, P.D., Bishnoi, P.R., 1997. Kinetics of carbon dioxide and methane hydrate formation. The Canadian Journal of Chemical Engineering 75(6), 1090-1099.
Mochizuki, T., Mori, Y.H., 2006. Clathrate-hydrate film growth along water/hydrate-former phase boundaries—numerical heat-transfer study. Journal of Crystal Growth 290(2), 642-652.
Mori, Y.H., 2001. Estimating the thickness of hydrate films from their lateral growth rates: application of a simplified heat transfer model. Journal of Crystal Growth 223(1), 206-212.
Mullin, J.W., 2001. Nucleation, Crystallization Butterworth-Heinemann, Oxford, pp. 181-215.
Natarajan, V., Bishnoi, P.R., Kalogerakis, N., 1994. Induction phenomena in gas hydrate nucleation. Chemical Engineering Science 49(13), 2075-2087.
Ou, W., Lu, W., Qu, K., Geng, L., Chou, I.M., 2016. In situ Raman spectroscopic investigation of flux-controlled crystal growth under high pressure: A case study of carbon dioxide hydrate growth in aqueous solution. International Journal of Heat and Mass Transfer 101, 834-843.
Radhakrishnan, R., Trout, B.L., 2002. A new approach for studying nucleation phenomena using molecular simulations: Application to $CO_2$ hydrate clathrates. The Journal of Chemical Physics 117(4), 1786-1796.
Ribeiro Jr, C.P., Lage, P.L.C., 2008. Modelling of hydrate formation kinetics: State-of-the-art and future directions. Chemical Engineering Science 63(8), 2007-2034.
Ripmeester, J.A., Alavi, S., 2016. Some current challenges in clathrate hydrate science: Nucleation, decomposition and the memory effect. Current Opinion in Solid State and Materials Science 20(6), 344-351.
Robinson, D.B., Peng, D.-Y., 1978. The characterization of the heptanes and heavier fractions for the GPA Peng-Robinson programs. Gas Processors Association, Tulsa, Okla.
Selim, M.S., Sloan, E.D., 1989. Heat and mass transfer during the dissociation of hydrates in porous media. AIChE Journal 35(6), 1049-1052.
Shi, B.-H., Fan, S.-S., Lou, X., 2014. Application of the shrinking-core model to the kinetics of repeated formation of methane hydrates in a system of mixed dry-water and porous hydrogel particulates. Chemical Engineering Science 109, 315-325.
Shi, B.-H., Gong, J., Sun, C.-Y., Zhao, J.-K., Ding, Y., Chen, G.-J., 2011. An inward and outward natural gas hydrates growth shell model considering intrinsic kinetics, mass and heat transfer. Chemical Engineering Journal 171(3), 1308-1316.
Shi, B.-H., Yang, L., Fan, S.-S., Lou, X., 2017. An investigation on repeated methane hydrates formation in porous hydrogel particles. Fuel 194, 395-405.
Skovborg, P., Ng, H.J., Rasmussen, P., Mohn, U., 1993. Measurement of induction times for the formation of methane and ethane gas hydrates. Chemical Engineering Science 48(3), 445-453.
Sloan, E.D., Koh, C.A., 2008. Clathraye Hydrates of Natural Gases, third ed. Taylor & Francis Group, New York.
Staykova, D.K., Kuhs, W.F., Salamatin, A.N., Hansen, T., 2003. Formation of porous gas hydrates from ice powders: Diffraction experiments and multistage model. The Journal of Physical Chemistry B 107(37), 10299-10311.
Sun, Q., Kang, Y.T., 2016. Review on $CO_2$ hydrate formation/dissociation and its cold energy application. Renewable and Sustainable Energy Reviews 62, 478-494.
Teng, H., Kinoshita, C.M., Masutani, S.M., 1995. Hydrate formation on the surface of a $CO_2$ droplet in high-pressure, low-temperature water. Chemical Engineering Science 50(4), 559-564.
Uchida, T., Ebinuma, T., Kawabata, J.i., Narita, H., 1999. Microscopic observations of formation processes of clathrate-hydrate films at an interface between water and carbon dioxide. Journal of Crystal Growth 204(3), 348-356.
Uddin, M., Coombe, D., Law, D., Gunter, B., 2008. Numerical studies of gas hydrate formation and decomposition in a geological reservoir. Journal of Energy Resources Technology 130(3), 032501-032501-032514.

1 Vatamanu, J., Kusalik, P.G., 2010. Observation of two-step nucleation in methane hydrates. Phys Chem
2 Chem Phys 12(45), 15065-15072.
3 Verrett, J., Servio, P., 2016. Reaction rate constant of $CO_2$-Tetra-n-butylammounium bromide semi-
4 clathrate formation. The Canadian Journal of Chemical Engineering 94(11), 2138-2144.
5 Vysniauskas, A., Bishnoi, P.R., 1983. A kinetic study of methane hydrate formation. Chemical
6 Engineering Science 38(7), 1061-1072.
7 Walsh, M.R., Beckham, G.T., Koh, C.A., Sloan, E.D., Wu, D.T., Sum, A.K., 2011. Methane hydrate
8 nucleation rates from molecular dynamics simulations: Effects of aqueous methane concentration,
9 interfacial curvature, and system size. The Journal of Physical Chemistry C 115(43), 21241-21248.
10 Yang, D., Le, L.A., Martinez, R.J., Currier, R.P., Spencer, D.F., 2011. Kinetics of $CO_2$ hydrate formation
11 in a continuous flow reactor. Chemical Engineering Journal 172(1), 144-157.
12 Yin, Z., Khurana, M., Tan, H.K., Linga, P., 2018. A review of gas hydrate growth kinetic models. Chemical
13 Engineering Journal 342, 9-29.

14

- A kinetic model is presented to observe features of the hydrate-based $CO_2$ capture.
- The model is able to predict the nucleation phase behavior and induction time.
- Temperature history profile over the nucleation and growth phases is simulated.
- The numerical estimation of the internal concentration profiles for a hydrating particle is demonstrated.
- A model-based criterion was proposed to estimate the nucleation number.

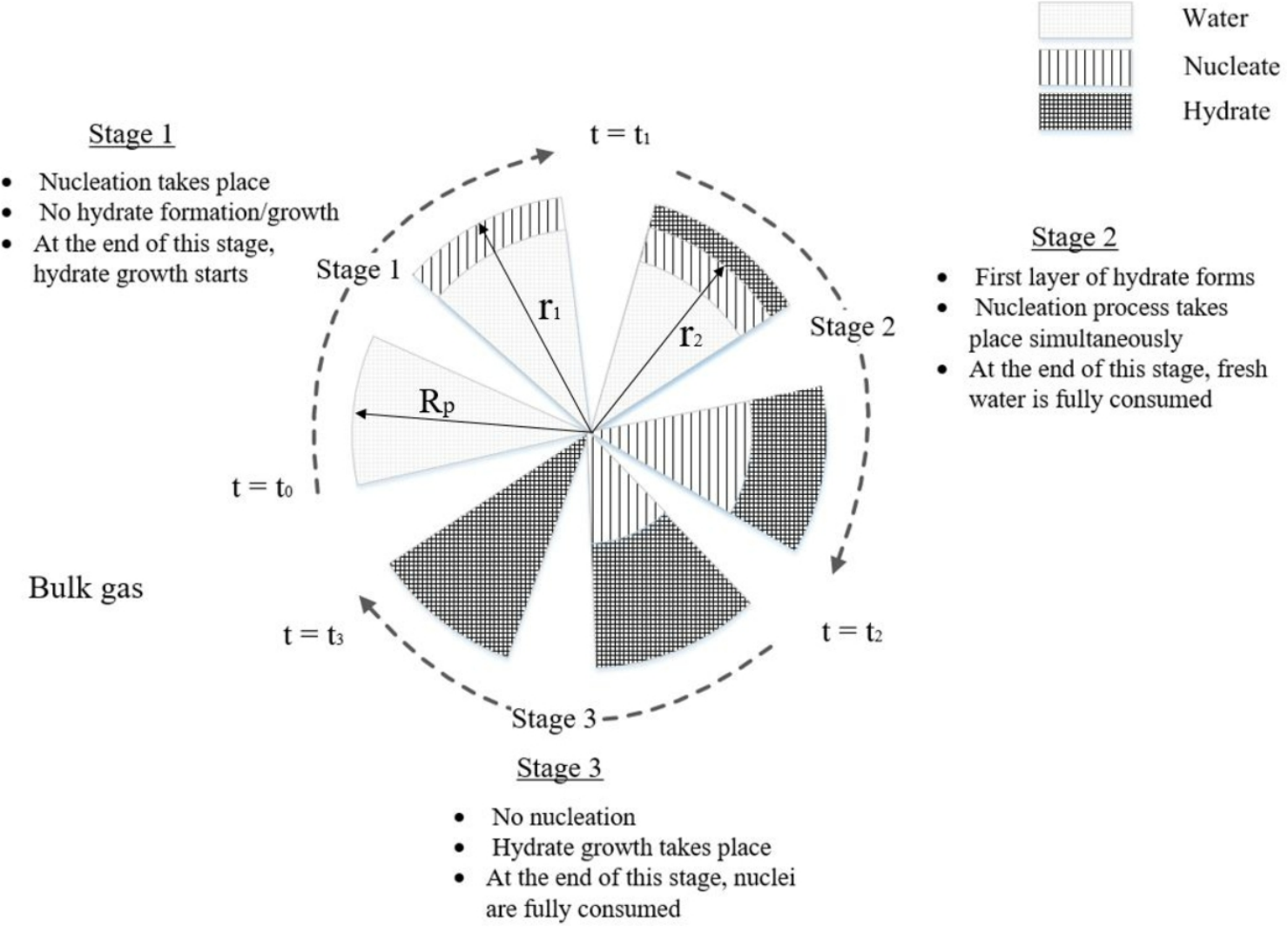
Water
Nucleate
Hydrate
Stage 1
Nucleation takes place
No hydrate formation/growth
At the end of this stage, hydrate growth starts
t = t1
Stage 1
r1
r2
Stage 2
Rp
t = t0
Bulk gas
t = t3
t = t2
Stage 3
Stage 2
First layer of hydrate forms
Nucleation process takes place simultaneously
At the end of this stage, fresh water is fully consumed
Stage 3
No nucleation
Hydrate growth takes place
At the end of this stage, nuclei are fully consumed